

The proton spin-dependent structure function g_2 at low Q^2

Ryan Zielinski*

The University of New Hampshire

E-mail: rbziel@jlab.org

While the neutron spin structure functions, g_1^n and g_2^n , and the longitudinal proton spin structure function, g_1^p , have been measured over a wide kinematic range, the second proton spin structure function, g_2^p , has not. This document will present the E08-027 (g_2^p) experiment, which was an inclusive measurement of g_2^p in the resonance region at Jefferson Lab's Hall A. This is the first measurement of g_2^p covering $0.02 \text{ GeV}^2 < Q^2 < 0.2 \text{ GeV}^2$. The experiment will allow us to test the Burkhardt-Cottingham Sum Rule at low Q^2 as well as extract the longitudinal-transverse generalized spin polarizability and compare it to predictions made by Chiral Perturbation Theory. In addition, the data will reduce the systematic uncertainty of calculations of the hyperfine splitting of hydrogen. An update on the status of the analysis, along with preliminary results, will be discussed.

*The 8th International Workshop on Chiral Dynamics, CD2015 ****

29 June 2015 - 03 July 2015

Pisa, Italy

*Speaker.

1. Introduction and Motivation

The nucleon is a composite system consisting of quarks and gluons that exhibit complex many-body interactions. The inclusive electron scattering process, $N(e, e^-)$, characterizes this deviation from point-like behavior with four structure functions, each describing a particular aspect of the nucleon's compositeness. These four can be subdivided into smaller groups of two, corresponding to the interaction of unpolarized (F_1 and F_2) and spin-polarized (g_1 and g_2) electrons and nucleons. The spin structure functions can be isolated by taking different combinations of beam and target polarizations, i.e. longitudinally polarized electrons with a longitudinally or transversely polarized nucleon,

$$\Delta\sigma_{\parallel} = \frac{d^2\sigma}{d\Omega dE'}(\downarrow\uparrow - \uparrow\uparrow) = \frac{4\alpha^2}{MQ^2} \frac{E'}{\nu E} \left[(E + E' \cos\theta) g_1(x, Q^2) - \frac{Q^2}{\nu} g_2(x, Q^2) \right], \quad (1.1)$$

$$\Delta\sigma_{\perp} = \frac{d^2\sigma}{d\Omega dE'}(\downarrow\Rightarrow - \uparrow\Rightarrow) = \frac{4\alpha^2 \sin\theta}{MQ^2} \frac{E'^2}{\nu^2 E} \left[\nu g_1(x, Q^2) - 2E g_2(x, Q^2) \right], \quad (1.2)$$

where ν is the energy transfer, θ is the scattering angle, Q^2 is the four-momentum transfer squared, α is the fine structure constant, M is the nucleon mass, x is the Bjorken scaling variable, and E and E' are the incident and outgoing electron energy, respectively. The electron spin is denoted by \uparrow and \downarrow and the nucleon spin by $\uparrow\uparrow$ and \Rightarrow .

While straightforward to measure experimentally, the current theories are unable to provide calculations of the structure functions from first principles. Instead, theoretical predictions of the moments of the structure functions, allow for comparison between experiment and theory. The moments are x -weighted integrals of the spin structure functions. The 0^{th} (no x -weighting) moment of the g_2 structure function is the Burkhardt-Cottingham (BC) sum rule [1],

$$\Gamma_2 = \int_0^1 g_2(x, Q^2) dx = 0. \quad (1.3)$$

Higher moments of the spin structure functions are related to electromagnetic polarizabilities by dispersive sum rules. There are several higher moments but these proceedings will focus on the longitudinal-transverse spin polarizability (δ_{LT}),

$$\delta_{LT}(Q^2) = \frac{16\alpha M^2}{Q^6} \int_0^{x_0} x^2 [g_1(x, Q^2) + g_2(x, Q^2)]. \quad (1.4)$$

A detailed experimental and theoretical background to the moments and sum rules of the spin structure functions is provided in Refs. [2, 3, 4].

Physical meaning can be attached to the structure functions by studying them in the Bjorken scaling limit; in Feynman's parton model, the structure functions F_1 , F_2 and g_1 are described as incoherent sums over the (non-interacting) parton momentum distribution functions. There is no simple interpretation of g_2 in the parton model, as its description necessarily includes contributions from quark-gluon interactions. Instead, turning to the operator product expansion, a non-zero g_2 is obtained using a twist expansion,

$$g_2(x, Q^2) = g_2^{\text{WW}}(x, Q^2) + \bar{g}_2(x, Q^2). \quad (1.5)$$

The leading twist term, g_2^{WW} , is defined completely by g_1 and is given by the Wandzura-Wilczek relation. The higher twist term, $\bar{g}_2(x, Q^2)$ is related to both the transverse polarization distribution of the quark and quark-gluon interactions. At smaller Q^2 , the higher twist term contributed more to g_2 , and low momentum transfer experimental measurements offer insight into the collective behavior of interacting partons within the nucleon.

At low momentum transfer the behavior of the structure functions is closely related to the global properties of the proton. Poor knowledge of the spin structure functions in the low Q^2 region has become a limiting factor in the precision of bound-state QED calculations. The energy levels in such systems can be measured to extremely high precision, so corresponding QED calculations have reached a level where the finite size of the nucleon as characterized by the structure functions is now the leading uncertainty. For example, hyperfine splitting in ground state hydrogen is measured at the 10^{-13} MHz level but only calculable to $\sim 10^{-6}$ MHz. The largest source of theoretical uncertainty is directly related to the structure functions. These proton structure corrections cannot be calculated directly from the fundamental theory, but are instead related to integrals of the measured structure functions. The current lack of g_2 measurements leads to a reliance on models to estimate its contribution [5, 6]. Currently the g_2 portion of the correction dominates the uncertainty, especially at the low momentum transfers that contribute the most (see Figure 1). The g_2 contribution is given by

$$\Delta_2 = -24m_p^2 \int_0^\infty \frac{dQ^2}{Q^4} B_2(Q^2), \quad (1.6)$$

$$B_2 = \int_0^{x_{th}} dx [1 + 2\tau - 2\sqrt{\tau(\tau+1)}] g_2(x, Q^2), \quad (1.7)$$

where $\tau = v^2/Q^2$ and x_{th} is the pion production threshold. The full hyperfine splitting calculation is detailed in Refs. [5, 6, 7, 8].

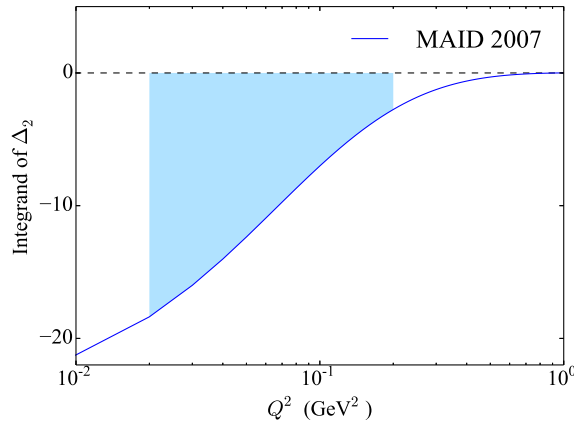


Figure 1: Low Q^2 dependence on the g_2 contribution to the structure corrections to the hydrogen hyperfine splitting. The blue shaded region represents the kinematic coverage of the g_2^p experiment.

2. Measurements of the Structure Functions

With the exception of g_2 of the proton, the four structure functions have been measured over a wide kinematic range for both the neutron and proton. The relative lack of g_2 structure function measurements is due to the technical difficulty in operating the required transversely polarized target. It is especially difficult for protons because a large (transverse) magnetic field is needed. The first dedicated measurement of proton g_2 was conducted at SLAC in E155x [9]. Their results are largely consistent with leading twist behavior, except for a 2.75σ discrepancy in their result for the BC sum rule. Although, that result has a large uncertainty, which is associated with extrapolation to the low- x portion of the integral.

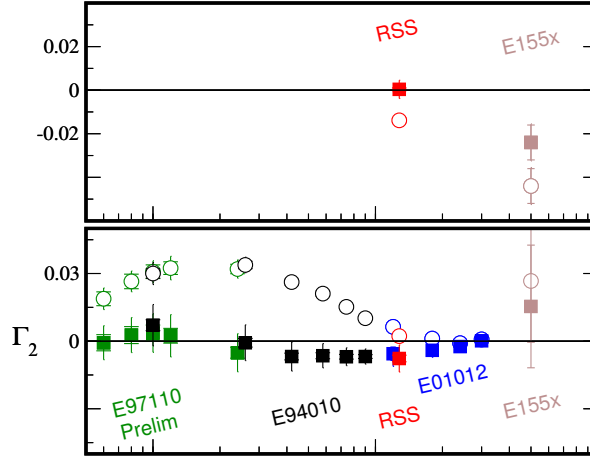


Figure 2: Current status of the BC sum rule [9, 10, 11, 12]. The top (bottom) plot are results on the proton (neutron). The open symbols represent the measured values and the solid symbols are the total sum rule, after including unmeasured contributions from the elastic and high-energy (low- x) region. Plot courtesy of K. Slifer [13].

Three Jefferson Lab (JLab) experiments followed E155x, covering a wide range of momentum transfer. The Resonance Spin Structure (RSS) experiment in Hall C measured g_2 of both the proton and deuteron in the resonance region at intermediate Q^2 [10]. They report results consistent with the BC sum rule, but the sum rule remains largely unmeasured for the proton. The current status of BC sum rule measurements is shown in Figure 2. The Spin Asymmetries of the Nucleon experiment (SANE), also performed in Hall C, provided a measurement of g_2^p in the high Q^2 region [14]. The most recent experiment, g_2^p , ran in Hall A and covered the low Q^2 region. The g_2^n structure function has also been extensively measured in Hall A [4].

The low momentum transfer g_2^p data is of particular interest because it covers a region not previously measured by E155x. The data is useful in testing Chiral Perturbation Theory (χ PT) calculations, which have shown inconsistency with the existing neutron data in terms of the longitudinal-transverse spin polarizability. The discrepancy is highlighted Figure 3, where the dotted blue line is the relativistic baryon χ PT prediction. The quantity δ_{LT} is thought to be a good testing ground for χ PT due to its insensitivity to the Δ -resonance. In addition, the integrals in the second moments, such as δ_{LT} , have a smaller contribution from the high- ν region and converge

much faster due to an extra $1/v^2$ weighting. This minimizes experimental uncertainty caused by the unmeasured region at large v . More recent calculations suggest better agreement [15], but there is still a lack of proton data.

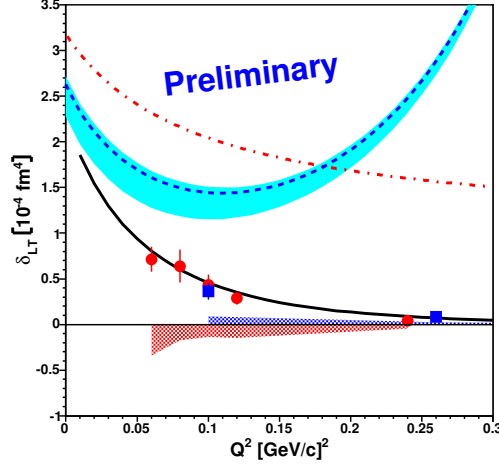


Figure 3: Neutron results for the longitudinal-transverse spin polarizability. The blue squares are published data from E94010 [16] and the red circles are preliminary data from E97110. The black line is the MAID prediction. Plot courtesy of V. Sulkosky [17].

3. The g_2^p Experiment

The g_2^p experiment successfully ran March to May 2012 in Hall A. We performed an inclusive measurement at forward angles of the proton spin-dependent cross sections in order to determine the g_2^p structure function and the longitudinal-transverse spin polarizability δ_{LT} in the resonance region for $0.02 < Q^2 < 0.20 \text{ GeV}^2$. A measurement of g_2 requires knowledge of both the parallel and perpendicular polarized cross sections. The experiment primarily measured the perpendicular contribution and will rely on the EG4 experiment from JLab's Hall B for the parallel component. Parallel data was taken at one setting to cross-check the EG4 results. The kinematic coverage of the experiment is shown in Figure 4.

The experiment required a large scale installation in Hall A (see Figure 5). To reach the lowest possible momentum transfer, a pair of room temperature septa magnets were installed at the entrance to the high resolution spectrometers (HRS) to allow detection of scattered electrons at 5.69° . Dynamical Nuclear Polarization (DNP) was used to polarize the solid ammonia target. The DNP target's strong magnetic field (5/2.5 T) required the installation of two large dipole magnets upstream of the target to provide chicaning of the beam. In order to limit depolarization of the polarized ammonia target, the experiment ran low currents (under 100 nA), which required the installation of new beam position monitors (BPMs) to fully characterize the beam profile. To further minimize depolarization, a slow raster was installed to raster the beam over the entire ~ 2 cm diameter target cup. The lower beam currents also led to the installation of a low current tungsten calorimeter to calibrate the beam current monitors (BCMs). At certain kinematics, a local beam dump collected the un-scattered beam.

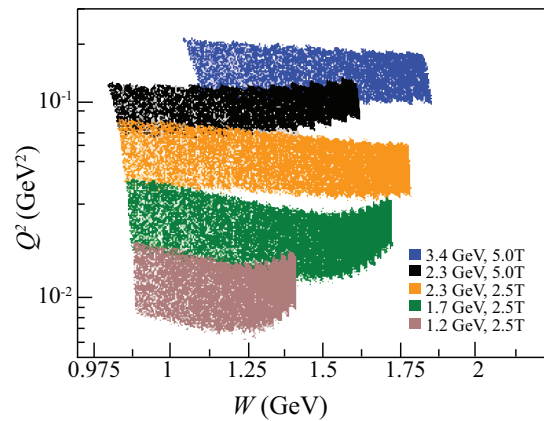


Figure 4: Kinematics covered during experimental run period. As W increases, Q^2 increases due to the target field creating a larger scattering angle.

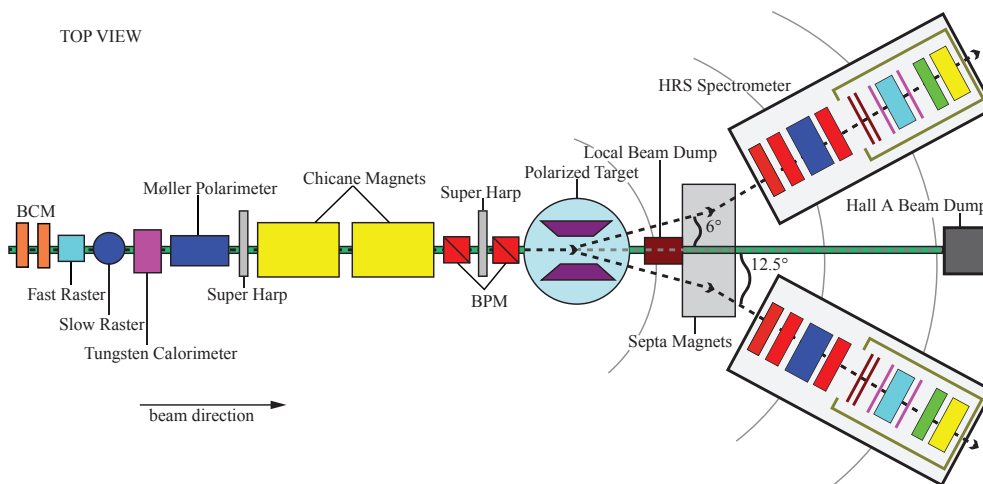


Figure 5: Hall A beamline for the g_2^p experiment.

The standard Hall A detector package was used in each HRS. Scattered electrons first passed through a pair of vertical drift wire-chambers (VDCs). The electrons ionized the gas inside the wire chambers and timing information from the ionization trail determined the position and angle of the trajectory. Next the electrons passed through a pair of segmented plastic scintillators approximately 2m apart, which formed the data acquisition trigger. Particle identification (PID) was provided by a gas Čerenkov detector and a two-layer electromagnetic calorimeter. The gas Čerenkov used the production of Čerenkov light in CO_2 to distinguish electrons from other negatively charged particles. The calorimeters used a collection of lead glass blocks to induce a cascade of pair production and bremsstrahlung radiation from energetic particles.

4. Status of the Analysis

Analysis of the g_2^p dataset is currently underway. The target polarization analysis is completed,

and polarizations averaged $\sim 70\%$ and $\sim 15\%$ for the 5T and 2.5T settings, respectively. The results are published in Ref. [18]. Detector calibration and efficiency studies have been completed for the PID and scintillator detectors. Multi-track and efficiency analysis of the VDC detectors is also complete. Scaler analysis to determine the BCM calibrations, helicity decoding and data-acquisition deadtime are finished. The optics analysis, which reconstructs the scattered electrons from the detector plane to the target, was made more difficult as compared to the standard HRS configuration by the large target field, septum field and chicane magnets. Although, the optics calibrations are now almost complete for the left HRS. Beam position and raster size calibrations have been completed and the results can be found in Ref. [19].

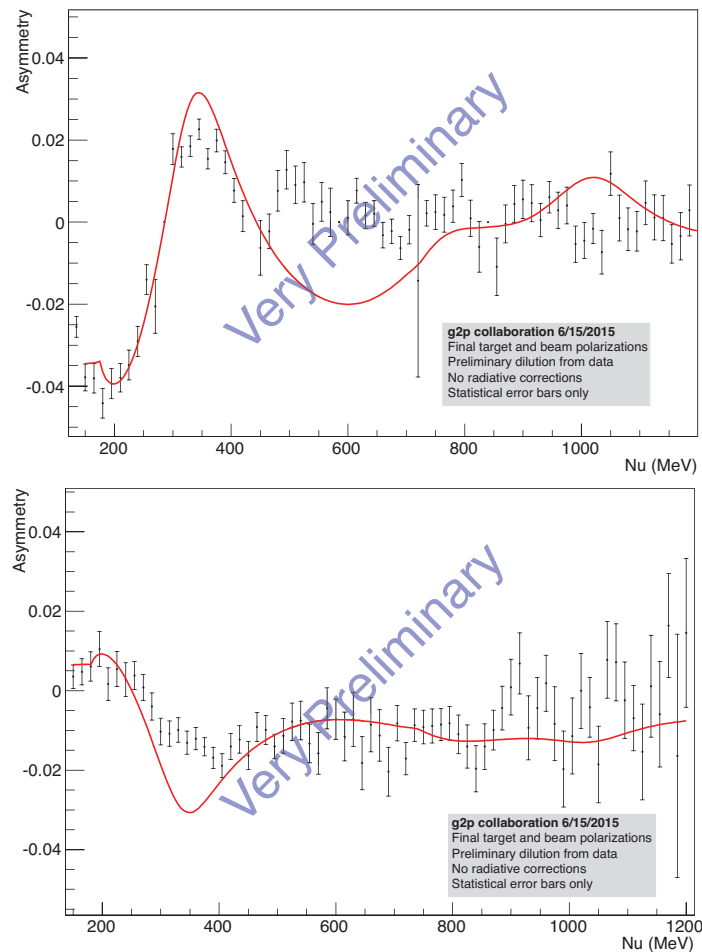


Figure 6: Experimental asymmetries for the 2254 MeV setting. The top (bottom) plot is the 5 T longitudinal (transverse) asymmetry. Plots courtesy of T. Badman.

Extraction of the relevant physics quantities requires removing the unpolarized and non-proton events from the measured cross sections and asymmetries. The fraction of protons within the target cup volume is determined in a packing fraction analysis, and the contribution from unpolarized background events, i.e. scattering from nitrogen, helium and the physical target cup, is determined in a dilution analysis, both of which are underway. In addition, a procedure to determine the spec-

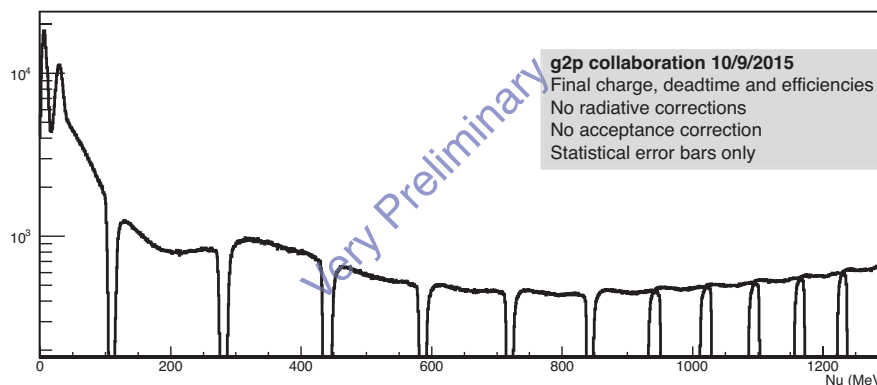


Figure 7: 2254 MeV normalized NH_3 yield (arb. units) for the 5 T longitudinal setting. Plot courtesy of T. Badman.

trometer acceptance is being developed, as well as a method to perform the radiative corrections to the cross sections (both polarized and unpolarized). Preliminary asymmetries and yields are shown in Figure 6 and Figure 7. The asymmetry has been scaled by the beam and target polarization, and dilution factor. The dilution factor used is a preliminary result based on data taken during the experiment on carbon, empty target cells and helium. The uncertainty in the asymmetry is purely statistical and it has not been radiatively corrected. The red line is a model prediction, where the radiated asymmetry is formed from the ratio of polarized cross sections from the MAID 2007 model [20] and the unpolarized cross sections from the empirical fit in Ref. [21]. The polarized model is radiated according to the formalism of Ref. [22] and the unpolarized to that of Ref. [23]. The yields show good separation between the nitrogen and hydrogen elastic peaks. A delta-resonance (Δ_{1232}) peak is also visible between $\nu = 200$ MeV and $\nu = 400$ MeV.

5. Summary

In these proceedings, we have discussed the measurements of the proton g_2 structure function. Jefferson Lab has been at the forefront of recent experimental developments with the RSS and SANE experiments providing measurements at intermediated and high momentum transfer. The gap in the low Q^2 coverage of g_2^p will be filled in by the recent g_2^p experiment. Poor knowledge of g_2^p is now a limiting factor in the precision of hydrogen hyperfine splitting calculations. The finite size of the nucleon, as characterized by the structure functions has become the leading uncertainty. Existing data has also revealed a striking discrepancy of χ PT calculations with the longitudinal-transverse spin polarizability δ_{LT}^n . These data will provide a benchmark test of χ PT and also allow a test of the BC sum rule at low Q^2 . Current results show that the sum rule is satisfied for the neutron but it is still largely unmeasured for the proton.

References

- [1] H. Burkhardt and W.N. Cottingham, *Ann. Phys. (N.Y.)* **56** (1970) 453.

- [2] J.-P. Chen, A. Deur and Z.-E. Meziani, *Mod. Phys. Lett. A* **20** (2005) 2745 [nucl-ex/0509007].
- [3] S. E. Kuhn, J.-P. Chen and E. Leader, *Prog. Part. Nucl. Phys.* **63** (2009) [hep-ph/08123535].
- [4] J.-P. Chen, *Int. J. Mod. Phys. E* **19** (2010) 1893 [nucl-ex/10013898].
- [5] V. Nazaryan, C.E. Carlson, K.A. Griffioen, *Phys. Rev. Lett.* **96** (2006) 163001 [hep-ph/0512108].
- [6] C.E. Carlson, V. Nazaryan, K. Griffioen, *Phys. Rev. A* **78** (2008) 022517.
- [7] A.V. Volotka, V.M. Shabaev, G. Plunien and G. Soff, *Eur. Phys. J. D* **33** (2005) 33.
- [8] A. Dupays, A. Beswick, B. Lepetit, C. Rizzo, and D. Bakalov, *Phys. Rev. A* **68** (2003) 052503.
- [9] P.L. Anthony *et al.* [SLAC E155 Collaboration] *Phys. Lett. B* **553** (2003) 18.
- [10] F.R. Wesselmann *et al.* [RSS Collaboration] *Phys. Rev. Lett.* **105** (2010) 101601.
- [11] P. Solvignon *et al.* [E01-012 Collaboration] *Phys. Rev. C* **92** (2015) 015208.
- [12] M. Amarian *et al.* [E94-010 Collaboration] *Phys. Rev. Lett.* **92** (2004) 022301.
- [13] K. Slifer, *AIP Conf. Proc.* **1149** (2009) 130.
- [14] S. Choi, M. Jones, Z. E. Meziani and O. Rondon-Aramayo, *Spin Asymmetries of the Nucleon Experiment*, Experimental Proposal (2006).
- [15] V. Lensky, J.M. Alarcón, V. Pascalutsa, *Phys. Rev. C* **90** (2014) 055202.
- [16] M. Amarian *et al.* [E94-010 Collaboration] *Phys. Rev. Lett.* **93** (2004). 152301.
- [17] V. Sulkosky, *PoS CD12* (2013) 023.
- [18] J. Pierce *et al.*, *Physics of Particles and Nuclei* **45** (2014) 303.
- [19] P. Zhu *et al.*, arXiv:1509.03510 [physics.ins-det] (2015).
- [20] D. Drechsel, S.S. Kamalov and L. Tiator, *Nucl. Phys. A* **645** (1999) 145.
- [21] M.E. Christy and P.B. Bosted, *Phys. Rev. C* **81** (2007) 055213.
- [22] I. Akushevich, A. Ilyichev and N. Shumeiko, arXiv:0106180 [hep-ph] (2001).
- [23] L.W. Mo and Y.S. Tsai, *Rev. Mod. Phys* **41** 1969 (2005).